OPEN ACCESS
JOURNAL OF ADVANCED DIELECTRICS
Vol. 11, No. 4 (2021) 2150015 (9 pages)

DOI: 10.1142/S2010135X21500156

# Dielectric, impedance, modulus spectroscopy and AC conductivity studies on novel organic ferroelectric diisopropylammonium chloride (dipaCl)

Mamataj Khatun* and Ekramul Kabir†,‡

*Department of Physics, Aliah University, Newtown Campus
Kolkata 700160, India

†Department of Physics, Darjeeling Govt. College
Darjeeling 734101, India

‡ekramulphysics@gmail.com

Received 26 March 2021; Revised 26 April 2021; Accepted 29 April 2021; Published 11 June 2021

Organic molecular ferroelectric diisopropylammonium chloride (dipaCl) was successfully synthesized using diisopropylamine, hydrochloric acid (57%) and methanol solution. Dielectric permittivity, impedance, modulus spectroscopy and conductivity were systematically studied by Capacitance–Conductance ($C_P - G$) measurements in the temperature range of 373–445 K. Dielectric property tests clearly show that the organic molecular ferroelectric dipaCl obeys Curies–Weiss law $1/\varepsilon = (T–T_0)/C$. The real ($Z'$) and imaginary ($Z''$) parts of the electrical modulus were calculated from the various values of $\varepsilon'$ and $\varepsilon''$. It is shown that AC conductivity satisfies the relation $\sigma(\omega) \infty \omega^n$, where the power exponent $n$ depends on temperature and frequency. From Arrhenius equation, the activation energies $E_\sigma$ and $E_h$ are also calculated which describes the complete conduction mechanism of dipaCl.

*Keywords*: Molecular ferroelectrics; dielectric spectroscopy; impedance spectroscopy; conductivity.

## 1. Introduction

Molecular ferroelectrics have been recently developed as an important complementary for the traditional inorganic counterparts as they have numerous advantages including multi-functionality, low density, low cost and solution processability which will make them suitable candidates for the development of all-organic electronics. In the past decades, organic ferroelectrics have attracted increasing attention because of their large number of potential applications, including memory chip, sensing, actuation, energy harvesting and fast switchable data storage, especially with respect to bionic devices.[1–7] Inorganic ferroelectric ionic perovskite oxides barium titanate and lead zirconate titanate are mainly used in numerous potential applications due to their high dielectric constant, high spontaneous polarization ($P_S$) and high ferroelectric–paraelectric transition temperature ($T_C$). But the limitations of having heavyweight, containing toxic lead and high-temperature processing lead the scientists to synthesize new organic ferroelectrics comparable to the high spontaneous polarization of perovskite oxides, high dielectric constant and with the transition temperature ($T_C$) well above room temperature processing. Recently, various room temperature organic ferroelectric materials such as diisopropylammonium chloride (dipaCl),[8–11] diisopropylammonium bromide (dipaBr)[12–17] and diisopropylammonium iodide (dipaI)[18–20] reveal high Curie temperatures (*Tc*) of 440 K, 425 K and 415 K, respectively, and possess large spontaneous polarization (Ps) of 8.9 $\mu$C/cm$^2$, 23 $\mu$C/cm$^2$ and 33 $\mu$C/cm$^2$, respectively, close to that of PVDF i.e., 8 $\mu$C/cm$^2$ and inorganic barium titanate ($BaTiO_3$) i.e., 26 $\mu$C/cm$^2$. However, there is some experimental controversy over dipaI about polarization and transition temperature.[18,21] Amongst them, dipaCl exhibits the highest transition temperature useful for practical applications such as in nonvolatile random access memory devices, automotive electronic devices, aerospace and power-generating industries which usually work under severe thermal conditions. In previous works, Fu *et al*. showed the study carried out on the structural, thermal and dielectric properties of dipaCl.[8] Looking at its application potential, it is imperative to investigate the electrical behavior including ac conductivity and dielectric properties with a view to understand the conduction mechanism involved in dipaCl in a wide frequency and temperature range.

## 2. Material and Methods

Diisopropylamine and hydrochloric acid (57%) were purchased from available sources. The solvent, methanol used for synthesis and recrystallization is of AR grade and used without further purification.

‡Corresponding author.

The crystalline samples of dipaCl were grown by slow evaporation of methanol solution containing equal molar amounts of diisopropylamine and hydrochloric acid. Small transparent crystals were formed after few days. The obtained polycrystalline material was further recrystallized in methanol solution at room temperature. The dielectric studies are performed on the pellet sample using an impedance analyzer Keysight E4990A.

## 3. Results and Discussion

### 3.1. *Dielectric studies*

Dielectric behavior of the material has been investigated by an impedance analyzer over a wide range of temperatures and frequencies. The dielectric permittivity was determined from the measured values of capacitance and conductance using the following relation[22]

$$\varepsilon(\omega) = \varepsilon'(\omega) + j\varepsilon''(\omega). \quad (1)$$

Physically, $\varepsilon'$ and $\varepsilon''$ represent the charging and the loss current, respectively, that are frequency and temperature-dependent.[23,24] The real part of the complex dielectric permittivity, the dielectric constant ($\varepsilon'$), of dipaCl was calculated using the relation[25,26]

$$\varepsilon'(\omega) = \frac{C_p(\omega)d}{\varepsilon_0 A}, \quad (2)$$

where $C_p$ is the measured value of capacitance in the strong accumulation region, corresponding to the material capacitance, $A$ is the contact area of the pellet, $d$ is the thickness and $\varepsilon_0$ is the permittivity of free space charge ($\varepsilon_0 = 8.85 \times 10^{-14}$ F/cm).

On the other hand, the imaginary part of the complex dielectric permittivity i.e., dielectric loss ($\varepsilon''$) was calculated using the measured conductance $G(\omega)$ values from the relation

$$\varepsilon'' = \frac{G(\omega)d}{\omega\varepsilon_0 A}. \quad (3)$$

The loss tangent ($\tan\delta$) can be expressed as follows:[25–27]

$$\tan\delta = \frac{\varepsilon''}{\varepsilon'}. \quad (4)$$

The frequency dependence of the real ($\varepsilon'$) and imaginary ($\varepsilon''$) part of the dielectric constant at different temperatures has been shown in Figs. 1(a) and 1(b). It is clear that $\varepsilon'$ follows an inverse dependence of frequency i.e., the dielectric constant decreases with the increase in frequency which is normally followed by all dielectrics and/or ferroelectrics materials. In the low-frequency region dispersion with a high dielectric constant can be seen and in the high-frequency region, dielectric constant decreases very sharply.[28–30] Similar to the behavior of dielectric constant with frequency is shown in $\varepsilon''$-log $f$ graph (Fig. 1(b)). The frequency dependences of the $\varepsilon'$ and $\varepsilon''$

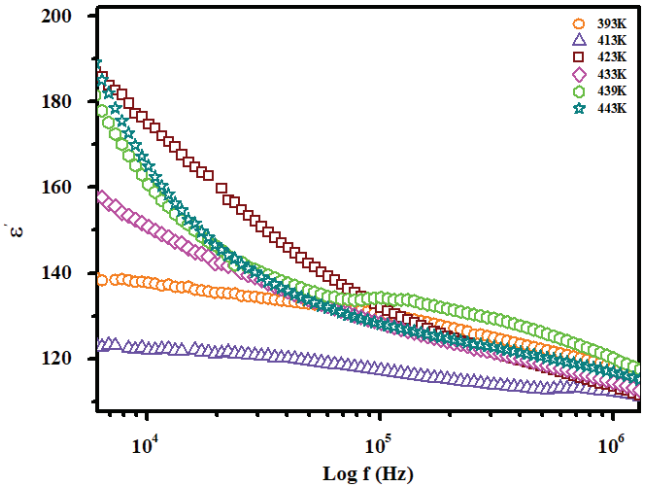


(a)

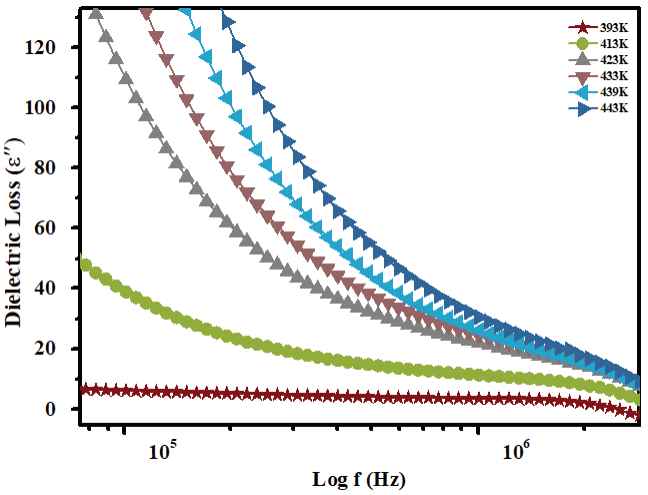


(b)

Fig. 1. (a) Frequency dependence of real part of permittivity ($\varepsilon'$) of dipaCl at various temperatures. (b) Frequency dependence imaginary part of permittivity ($\varepsilon''$) of dipaCl at various temperatures.

are probably related to the presence of an interfacial surface, resulting in an undesirable Maxwell–Wagner-type dispersion in the dielectric data. As the frequency is raised, the interfacial dipoles have less time to orient themselves in the direction of the alternating field and thus results in decrease in $\varepsilon'$ and $\varepsilon''$ with the increasing frequency. The charges can no longer follow the field with the increase in frequency and their contribution to the dielectric constant ceases.[31–36]

A varying field will alter this energy difference thus producing a net polarization. This part of the polarization, which is not in phase with the applied electric field, is defined as dielectric loss.[37] In this study of dielectric loss, it is familiar that at low frequencies, the high dielectric loss occurs due to the space charge polarization and at higher frequencies, the dielectric loss decreases, as a result, the electrical

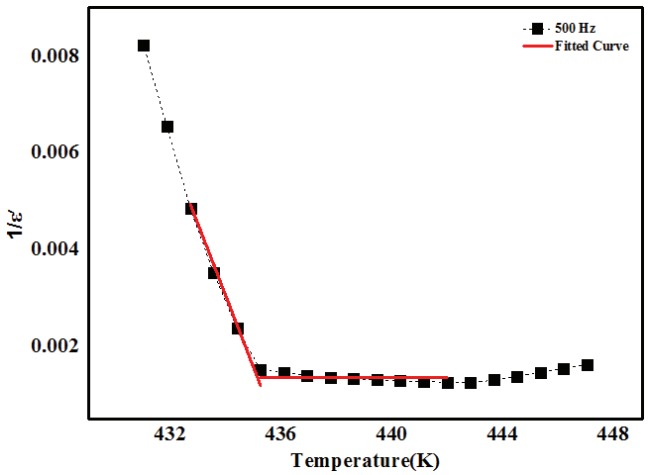


Fig. 2. Plot of $1/\varepsilon$ versus temperature, fitted curve satisfied Curie–Weiss law.

conductivity of the sample increases. From this figure, it can also be concluded that with the rise in temperature, dielectric loss also increases.

Previous dielectric studies[8] of the material reported that the transition temperature ($T_C$) is 442 K which is in good agreement with our experimental result and also $1/\varepsilon'$ – T data are well fitted with the curie-Weiss law which is shown in Fig. 2.

### 3.2. *Complex impedance analysis*

The electrical properties of the material have been investigated by impedance spectroscopy in a wide range of frequencies and temperatures. To analyze the microstructure and properties relationship of the material, impedance spectroscopy is a very powerful technique. The real part and the imaginary part of complex impedance are given by the following relations:

$$Z' = G/(G^2+\omega^2 C_P^2), \tag{5}$$

and

$$Z''=\omega C_P/(G^2+\omega^2 C_P^2). \tag{6}$$

The variation of real ($Z'$) and imaginary ($Z''$) part of impedance with frequency ($f$) at different temperatures are plotted in Figs. 3(a) and 3(b). It is observed from Figs. 3(a) and 3(b) that the magnitude of $Z'$ and $Z''$ decreases with increasing frequency and temperature and also merges at high frequency (>100 kHz). From the close investigation of these two curves, it can be concluded that with the increase in frequency and temperature in the higher frequency region, the two curves achieve a very low constant value, and the ac conductivity increases due to the removal of space charge. At lower frequency region, the values of both $Z'$ and $Z''$

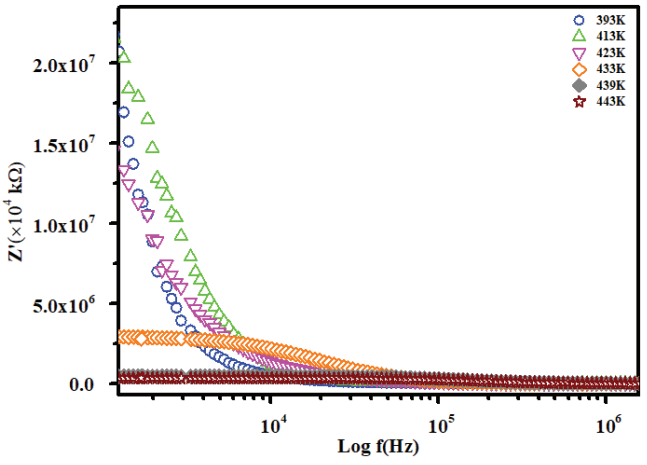


(a)

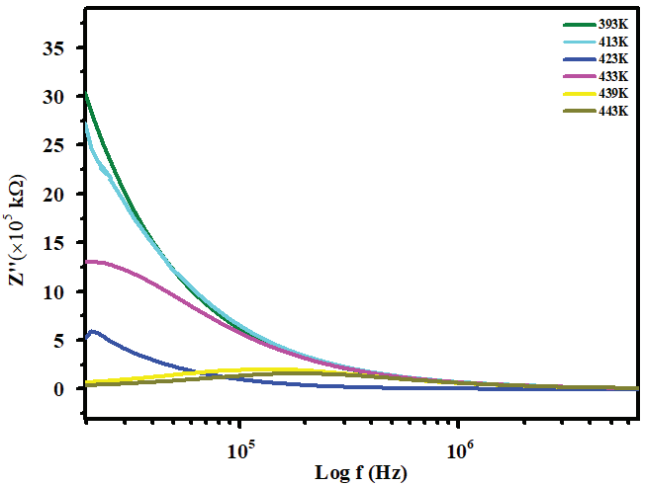


(b)

Fig. 3. (a) Frequency dependence of real part of impedance ($Z'$) of dipaCl at various temperatures. (b) Frequency dependence of imaginary part of impedance ($Z''$) of dipaCl at various temperatures.

decrease with the increase in temperature which indicates negative temperature coefficient resistance similar to that of semiconductors.[38,39] The impedance spectroscopy analysis result which is performed at different temperatures on dipaCl is presented in Fig. 4. From this figure, it can be seen that for lower temperature measurements, there is no semicircular curve but at higher temperature, $Z''$ versus $Z'$ curve changes and it comprises of semicircular arcs indicating that the conductivity increases with the rise of temperature. Here, the relaxation mechanism of dipaCl is due to only the grain (bulk) effect because the single semicircular arc passing through the origin of the entire frequency region of all temperatures. These figures also indicate that the endpoints of the semicircular arcs lie on the real $Z$-axis and the center lies below this axis reveals that the relaxations in dipaCl is of nondebye type.

Using impedance spectra, the physical process which occurs inside the material can be modeled as an equivalent

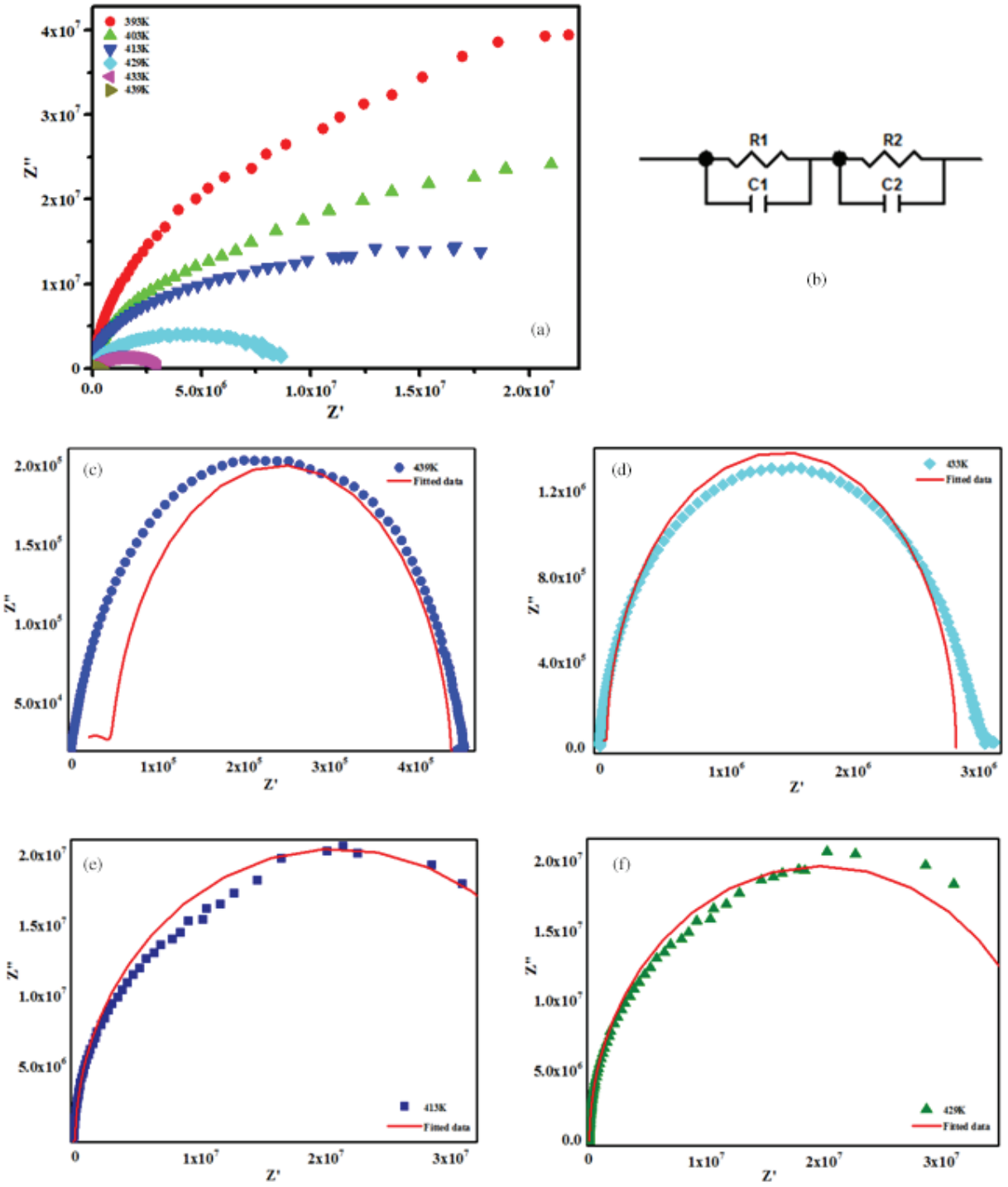


Fig. 4. (a) Nyquist plot ($Z'$ versus $Z''$) of dipaCl at different temperatures, (b) Equivalent circuit, (c) Fitted Nyquist plot at temperature 439 K, (d) Fitted Nyquist plot at temperature 433 K, (e) Fitted Nyquist plot at temperature 413 K and (f) Fitted Nyquist plot at temperature 429 K.

circuit. After a careful investigation, by fitting the impedance data from the complex impedance spectra, one can obtain an appropriate equivalent circuit with information about the resistance and capacitance of the component. This simple common model comprising of two parallel RC circuits is connected in the series. The representation of any material through an electrical circuit analog is very helpful in representing the electrical features of the material. The real part

Table 1. The resistance and capacitance values of the equivalent circuit at different temperatures.

| Temp T(K) | $R_1 \times 10^4$ (Ω) | $C_1$ (pf) | $R_2 \times 10^6$ (Ω) | $C_2$ (pf) |
|---|---|---|---|---|
| 439 | 4.83 | 3.57 | 0.39 | 45.43 |
| 433 | 5.29 | 2.78 | 2.76 | 21.78 |
| 429 | 6.95 | 2.61 | 39.40 | 16.15 |
| 413 | 16.40 | 2.14 | 41.70 | 8.54 |

and complex part of the impedance can be obtained from the equivalent circuit by the following relations:[40]

$$Z' = \frac{R_1}{1+(\omega R_1 C_1)^2} + \frac{R_2}{1+(\omega R_2 C_2)^2}, \quad (7)$$

and

$$Z'' = \frac{R_1^2 \omega C_1}{1+(\omega R_1 C_1)^2} + \frac{R_2^2 \omega C_1}{1+(\omega R_2 C_2)^2}. \quad (8)$$

From the micro-structural point of view, a ferroelectric material is composed of grains and grain boundaries, exhibiting different dielectric permittivity ($\varepsilon$). So, here, $R_1$ and $C_1$ correspond to the resistance and capacitance of the grain, while $R_2$ and $C_2$ are the resistance and capacitance of the grain boundary, respectively.

In Table 1, the RC parameters which are obtained from fitting the complex impedance plot are shown.

### 3.3. *Complex modulus analysis*

At first, the dielectric modulus formalism was introduced to study the dielectric response of nonconducting materials, but afterward, it was also used in polymers and polymers composite materials. The modulus presents the real dielectric relaxation process and the relaxation behavior has been demonstrated by using the modulus formalism.[41–43] The electric modulus $M$ is expressed in the complex modulus formulism as follows:

$$M = \frac{1}{\varepsilon} = M' + jM'' = j\omega\varepsilon_0 Z, \quad (9)$$

where $M' = \omega C_0 Z''$ and $M'' = \omega C_0 Z'$ ($\omega$ = angular frequency ($2\pi f$)), $C_0$ = Geometrical capacitance = $\varepsilon_0$ (A/d).

The real part ($M'$) and the imaginary part ($M''$) of the complex electric modulus ($M$) can be expressed as follows:

$$M' = \frac{\varepsilon'}{(\varepsilon')^2 + (\varepsilon'')^2}, \quad (10)$$

and

$$M'' = \frac{\varepsilon''}{(\varepsilon')^2 + (\varepsilon'')^2}. \quad (11)$$

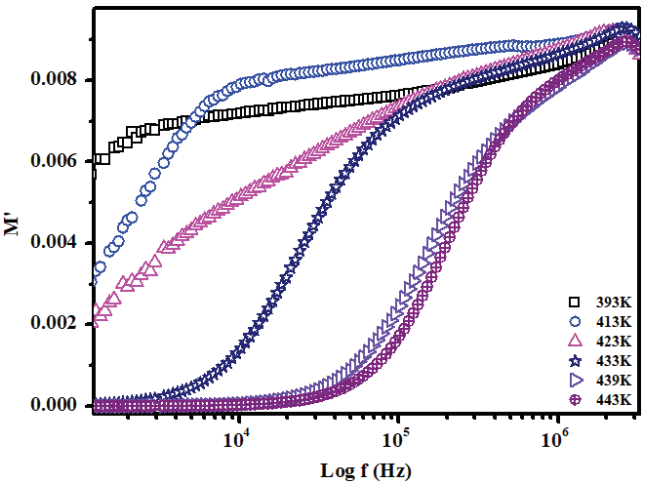


(a)

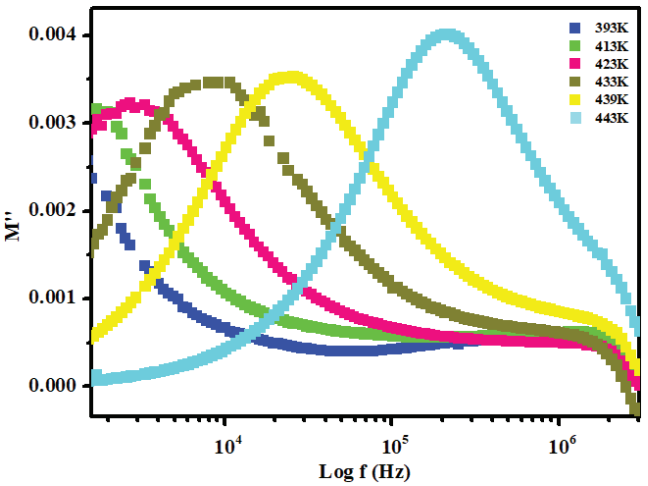


(b)

Fig. 5. (a) Frequency dependence of real part of modulus ($M'$) at different temperatures. (b) Frequency dependence of imaginary part of modulus ($M''$) at different temperatures.

The real component $M'$ and the imaginary component $M''$ were calculated from $\varepsilon'$ and $\varepsilon''$.

Figures 5(a) and 5(b) show the variation of real ($M'$) and imaginary ($M''$) part of modulus with frequency at different temperatures. It is clear from the figure that the value of $M'$ rises gradually with the rise in temperature and at low frequency $M'$ attains a very lower value but increases very sharply with the rise in frequency and attains a saturated value which increases with increase in temperature. This confirms the nonexistence of a substantial electrode polarization which is related to the frequency-independent electrical properties of the dielectric materials. The graph $M''$ – log $f$ indicates that below peak frequency ($f_{max}$) range, the charge carriers are mobile over the long distances and the peaks are shifted towards higher frequency sides with increasing temperatures. Here, the variation of modulus peak ($M''_{max}$) and

$f_{max}$ indicates that the variation is due to the capacitance (C). On increasing frequency, with the increase in the modulus peak indicates that at higher frequency range, the capacitance value decreases. The ions are capable of moving long distances at the low-frequency side but at the high-frequency side, the ions are confined to their potential wells.[44,45]

### 3.4. *Electrical conductivity analysis*

The frequency-dependent ac conductivity ($\sigma_{ac}$) can be obtained from the dielectric losses according to the following relation[36,46–51]:

$$\sigma = j\varepsilon_0\omega\varepsilon = j\varepsilon_0\omega(\varepsilon' - j\varepsilon'') = \varepsilon_0\omega\varepsilon'' - j\varepsilon_0\omega\varepsilon'. \quad (12)$$

The real part of complex conductivity ($\sigma_{ac}$) is calculated using the relation

$$\sigma_{ac} = \omega\varepsilon_0\varepsilon' \tan\delta = \omega\varepsilon_0\varepsilon''. \quad (13)$$

Figure 6 illustrates the frequency dependence of ac conductivity at different temperatures. In the lower frequency region ($\omega < \omega_h$), the conductivity is found to be frequency independent which suggests that the ions move in forward–backward direction.[52] Conductivity increases with frequency obeying the power dispersion law $\sigma(\omega) \infty \omega^n$ when the frequency exceeds hopping frequency ($\omega_h$). The ac conductivity behavior can be explained by Jonscher's power law equation i.e., universal power law (UPL)[53]:

$$\sigma(\omega) = \sigma_{dc} + A\omega^n \quad (0 < n < 1), \quad (14)$$

$$= \sigma_{dc} + \left[1 + \left(\frac{\omega}{\omega_p}\right)^n\right]. \quad (15)$$

Table 2. Comparison of electrical parameters of dipaCl at different temperatures.

| Temperature (K) | DC conductivity ($\sigma_{dc}$) | $n$ | Hopping frequency ($\omega_h$) |
|---|---|---|---|
| 409 | $1.88 \times 10^{-5}$ | 0.89 | 4644.1 |
| 429 | $5.74 \times 10^{-5}$ | 0.83 | 26392.89 |
| 433 | $1.70 \times 10^{-4}$ | 0.79 | 77494.40 |
| 435 | $5.40 \times 10^{-4}$ | 0.74 | 132788.97 |
| 439 | $9.60 \times 10^{-4}$ | 0.70 | 400271.532 |

Here, $n$ is the power of exponent, $A$ and $n$ are the thermally activated quantities. AC conductivity spectra at different temperatures are fitted (continuous line is shown in the figure) with the power-law equation and extracted the several parameters $\sigma_{dc}$, $\omega_h$ and $n$ which are shown in Table 2.

Here, $n$ represents the information about the type of conduction mechanism of the material and the values of exponent $n$ are always less than 1 for different temperatures and decreases with increase in temperature as shown in Fig. 7.

This model is based on hopping of charge carriers over the potential barrier (predicts a decrease of the value of $n$ with an increase in temperature) and this is consistent with the experimental results.[54–56] The variation of $\sigma_{dc}$, $\omega_h$ and $n$ with temperature is shown in Fig. 8. Usually, the parameters $\sigma_{dc}$ and $\omega_h$ are strongly temperature-dependent. Such dependency is fitted with the Arrhenius equation[57,58]

$$\sigma_{dc} = \sigma_0 \exp\left(-\frac{E_\sigma}{K_B T}\right), \quad (16)$$

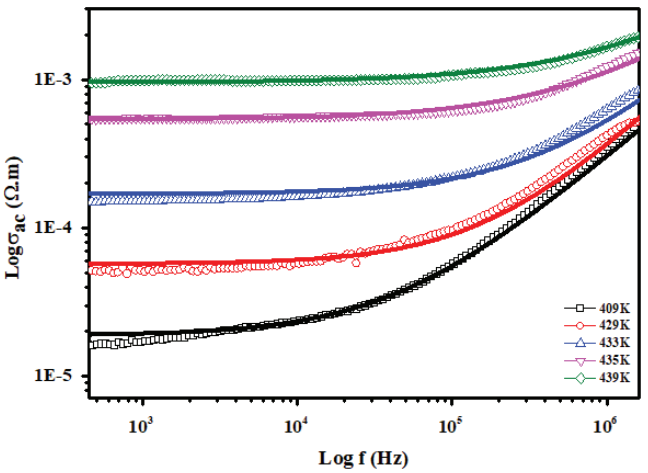


Fig. 6. Experimental and fitted curve of AC conductivity as a function of frequency for different temperatures.

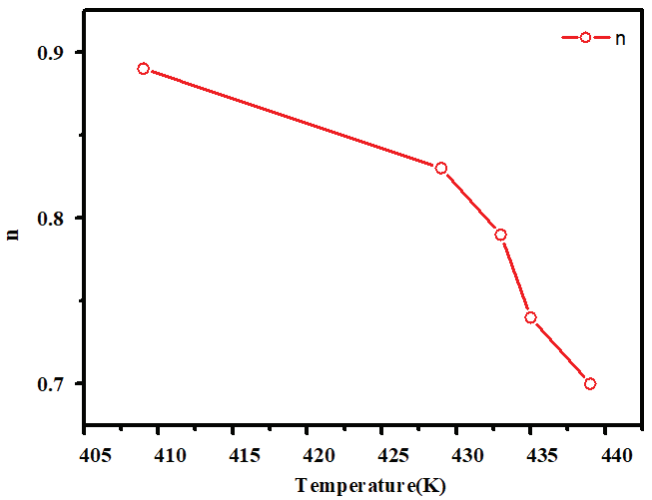


Fig. 7. Variation of $n$ with temperature.

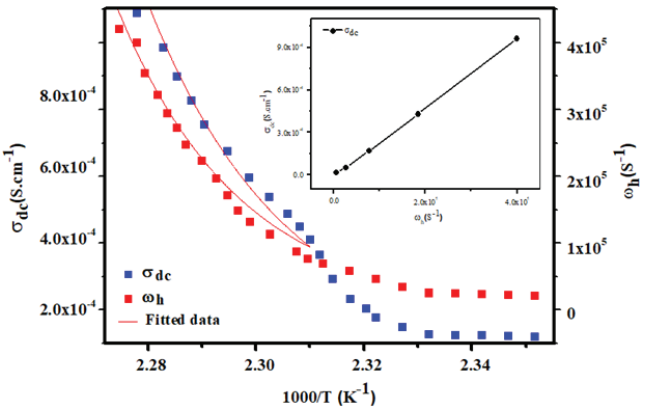


Fig. 8. Variation of hoping frequency $\omega_h$ and dc conductivity $\sigma_{dc}$ as a function of temperature. Solids lines represent the fit of experimental data. For ionic conduction, $\sigma_{dc}$ and $\omega_h$ satisfies the Barton–Nakajima–Namikawa.

and

$$\omega_h = \omega_{h0} \exp\left(-\frac{E_h}{K_B T}\right). \quad (17)$$

Here, $\sigma_0$ is the dc conductivity pre-exponential factor, $K_B$ denotes the Boltzman constant, $E_\sigma$ denotes the dc conductivity activation energy, $\omega_{h0}$ denotes the pre-exponential of hopping frequency and $E_h$ denotes the activation energy for hopping frequency. From the fitted curve, we get the activation energy $E_\sigma = 1.02$ eV and $E_h = 1.13$ eV. From the value of activation energies, it is clear that the activation energies are very close to each other within experimental error due to the fact that the charge carriers have to overcome the same energy barrier while conducting as well as relaxing.

## 4. Conclusions

In conclusion, this work has demonstrated that the new novel organic molecular ferroelectric dipaCl is a very interesting candidate with high spontaneous polarization and high dielectric constant. This paper summarizes the temperature and frequency dependence of the dielectric modulus, dielectric permittivity, complex impedance and ac conductivity of this green ferroelectric material. From the dielectric analysis, it can be concluded that at the higher frequency zone, the dielectric loss decreases and simultaneously the conductivity of the sample increases. The frequency dependences of the $\varepsilon'$ and $\varepsilon''$ are probably related to the presence of an interfacial surface, resulting in an undesirable Maxwell–Wagner-type dispersion in the dielectric data. From Nyquist plot, it is concluded that the relaxations in dipaCl is of nondebye type. With increasing frequency and temperatures, the value of ac conductivity increases. Here, the conduction mechanism was suggested to be hopping type of conduction due to the presence of a very small value of activation energies ($E_\sigma = 1.02$ eV and $E_h = 1.13$ eV). From the conductivity measurement, it is clear that the activation energies are very close to each other within experimental error due to the fact that the charge carriers have to overcome the same energy barrier while conducting as well as relaxing. Here, the ac conductivity is found to follow the universal power-law which can be explained by the correlated barrier hopping model (CBM).

## References

[1]C. A. Paz de Araujo and G. W. Taylor, *Ferroelectrics* **116**, 215 (2011).
[2]H. Y. Ye, Y. Zhang, S. Noro, K. Kubo, M. Yoshitake, Z. Q. Liu, H. L. Cai, D. W. Fu, H. Yoshikawa, K. Awaga, R. G. Xiong and T. Nakamura, Molecule-displacive ferroelectricity in organic supramolecular solids, *Sci. Rep*. **3**, 2249 (2013).
[3]C. R. Bowen, J. Taylor, E. LeBoulbar, D. Zabek, A. Chauhan and R. Vaish, Pyroelectric materials and devices for energy harvesting applications, *Energy Environ. Sci*. **7**, 3836 (2014).
[4]H. Anetai, K. Sambe, T. Takeda, N. Hoshino and T. Akutagawa, Nanoscale effects in one-dimensional columnar supramolecular ferroelectrics, *Chem.-A Eur. J.* **25**, 11233 (2019).
[5]K. Gao, M. Gu, X. Qiu, X. N. Ying, H. Y. Ye, Y. Zhang, J. Sun, X. Meng, F. M. Zhang, D. Wu, H. L. Cai and X. S. Wu, Above-room-temperature molecular ferroelectric and fast switchable dielectric of diisopropylammonium perchlorate, *J. Mater. Chem. C* **2**, 9957 (2014).
[6]J. F. Scott, Applications of modern ferroelectrics, *Science* **315**, 954 (2007).
[7]H. Zhu, C. Fu and M. Mitsuishi, Organic ferroelectric field-effect transistor memories with poly(vinylidene fluoride) gate insulators and conjugated semiconductor channels: A review, *Poly. Int.* **70**, 404 (2021).
[8]D. W. Fu, W. Zhang, H. L. Cai, J. Z. Ge, Y. Zhang and R. G. Xiong, Diisopropylammonium chloride: A ferroelectric organic salt with a high phase transition temperature and practical utilization level of spontaneous polarization, *Adv. Mater.* **23**, 5658 (2011).
[9]S. V. Baryshnikov, E. V. Charnaya, A. Y. Milinskiy, V. A. Parfenov and I. V. Egorova, Impact of nanoconfinement on the diisopropylammonium chloride ($C_6H_{16}ClN$) organic ferroelectric, *Phase Trans.* **91**, 293 (2018).
[10]N. I. Uskova, E. V. Charnaya, D. Yu. Podorozhkin, S. V. Baryshnikov, I. V. Egorova and A. Y. Milinskiy, Structural evolution of diisopropylammonium chloride (DIPAC) molecular ferroelectric, *Phys. Solid State* **62**, 1195 (2020).
[11]S. Pongiappan and S. Karuppannan, Crystal structure, hirshfeld surface analysis and phase transformation behavior of diisopropylammonium chloride hemihydrate crystals, *J. Phys. Chem. Solids* **153**, 110008 (2021).
[12]D. W. Fu, H. L. Cai, Y. Liu, Q. Ye, W. Zhang, Y. Zhang, X. Y. Chen, G. Giovannetti, M. Capone, J. Li and R. G. Xiong, Diisopropylammonium bromide is a high-temperature molecular ferroelectric crystal, *Science* **339**, 425 (2013).
[13]A. Piecha, A. Gagor, R. Jakubas and P. Szklarz, Room-temperature ferroelectricity in diisopropylammonium bromide, *Cryst. Eng. Commun.* **15**, 940 (2013).
[14]G. Kociok-Kohn, B. Lungwitz and A. C. Filippou, Diisopropylammonium bromide, *Acta Cryst. C* **52**, 2309 (1996).
[15]K. Gao, C. Liu, Z. Cui, J. Zhu, H. L. Cai and X. S. Wu, Room-temperature growth of ferroelectric diisopropylammonium bromide with 12-crown-4 addition, *Cryst. Eng. Commun*. **17**, 2429 (2015).

[16]S. V. Baryshnikov, A. Y. Milinskii, E. V. Charnaya and I. V. Egorova, Size effect in nanocomposites based on molecular ferroelectric diisopropylammonium bromide, *Phys. Solid State* **61**, 134 (2019).
[17]S. Sahoo, T. R. Ravindran, V. Srihari, K. K. Pandey, S. Chandra, C. Thirmal and P. Murugavel, Pressure induced phase transformations in diisopropylammonium bromide, *J. Solid State Chem*. **274**, 182 (2019).
[18]R. K. Saripalli, D. Swain, S. Prasad, H. Nhalil, H. L. Bhat, T. N. G. Row and S. Elizabeth, Observation of ferroelectric phase and large spontaneous electric polarization in organic salt of diisopropylammonium iodide, *J. Appl. Phys*. **121**, 114101 (2017).
[19]E. Kabir *et al*., Complex impedance studies of organic ferroelectric- Diisopropylammonium Iodide (DIPAI), *AIP Conf. Pro*. **2142**, 040006 (2019).
[20] A. Y. Milinskiy, S. V. Baryshnikov, I. V. Egorova and H. T. Nguyen, Dielectric properties of ferroelectric diisopropylammonium iodide, *Phase Trans.* **92**, 406 (2019).
[21]A. Piecha-Bisiorek, A. Gagor, D. Isakov, P. Zielinski, M. Galazka and R. Jakubas, Phase sequence in diisopropylammonium iodide: Avoided ferroelectricity by the appearance of a reconstructed phase, *Inorg. Chem. Front*. **4**, 553 (2017).
[22]D. K. Pradhan, R. N. P. Choudhary and B. K. Samantaray, Studies of dielectric relaxation and AC conductivity behavior of plasticized polymer nanocomposite electrolytes, *Int. J. Electrochem. Sci*. **3**, 597 (2008).
[23]A. Eroğlu, A. Tataroğlu and S. Altındal, On the temperature dependent dielectric properties, conductivity and resistivity of MIS structures at 1 MHz, *Microelectron. Eng*. **91**, 154 (2012).
[24]M. M. Abdel Kader, M. Y. Elzayat, T. R. Hammad, A. I. Aboud and H. Abdelmonem, Dielectric permittivity, ac conductivity and phase transition in hydroxyl ammonium sulphate, *Phys. Scr*. **83**, 035705 (2011).
[25]A. Chelkowski, *Dielectric Physics* (Elsevier North-Holland, Amsterdam, 1980).
[26]M. Popescu and I. Bunget, *Physics of Solid Dielectrics* (Elsevier, Amsterdam, New York, 1984).
[27]A. Tataroğlu, Frequency and voltage dependence of the electrical and dielectric properties of Au/n-Si Schottky diodes with $SiO_2$ insulator layer, *J. Optoelectron. Adv. Mater*. **13**, 940 (2011).
[28]D. Kobor, O. Bodian, W. Bodian and A. K. Diallo, Structural and impedance characterization of ceramics prepared from NPK fertilizer, *Process. Appl. Ceram*. **9**, 107 (2015).
[29]J. Tellier, Ph. Boullay, D. B. Jennet and D. Mercuri, Structure versus relaxor properties in Aurivillius type compounds, *J. Eur. Ceram. Soc*. **27**, 3687 (2007).
[30] V. Purohit, R. N. P. Choudhary and A. Sahoo, Investigation of structure, microstructure, impedance, dielectric and transport properties of sodium tungstate titanate: $Na(W_{1/2}Ti_{1/2})O_3$, *Mater. Res. Exp*. **6**, 125710 (2019).
[31]S. Maity, D. Bhattacharya and S. K. Ray, Structural and impedance spectroscopy of pseudo-co-ablated $(SrBi_2Ta_2O_9)$-$(1-x)$–$(La_{0.67}Sr_{0.33}MnO_3)$ $x$ composites, *J. Phys. D: Appl. Phys*. **44**, 095403 (2011).
[32]Mubasher and M. Mumtaz, Nanocomposites of multi-walled carbon nanotubes/cobalt ferrite Nanoparticles: Synthesis, structural, dielectric and impedance spectroscopy, *J. Alloys Compd*. **866**, 158750 (2021).
[33]N. Singh, A. Agarwal and S. Sanghi, Dielectric relaxation, conductivity behavior and magnetic properties of Mg substituted Zn–Li ferrites, *Current Appl. Phys*. **11**, 783 (2011).
[34]E. B. Araújo and J. A. Eiras, Synthesis and characterization of thin films of $Bi_4Ti_3O_{12}$ from oxide precursors, *J. Phys. D: Appl. Phys*. **32**, 957 (1999).
[35]A. Tripathy, S. N. Das, S. K. Pradhan, S. Bhuyan and R. N. P. Choudhary, Temperature and frequency dependent dielectric and impedance characteristics of double perovskite $Bi_2MnCoO_6$ electronic material, *J. Mater. Sci. Mater. Electron.* **29**, 4770 (2018).
[36]A. K. Dubey, P. Singh, S. Singh, D. Kumar and O. Parkash, Charge compensation, electrical and dielectric behavior of lanthanum doped $CaCu_3Ti_4O_{12}$, *J. Alloys Compd*. **509**, 3899 (2011).
[37]L. Kungumadevi, R. Sathyamoorthy and A. Subbarayan, AC conductivity and dielectric properties of thermally evaporated PbTe thin films, *Solid-State Electron*. **54**, 58 (2010).
[38]A. Rouahi, A. Kahouli, F. Challali *et al*., Impedance and electric modulus study of amorphous TiTaO thin films: Highlight of the interphase effect, *J. Phys. D: Appl. Phys*. **46**, 065308 (2013).
[39]E. V. Hauff, Impedance spectroscopy for emerging photovoltaics, *J. Phys. Chem. C* **123**, 11329 (2019).
[40]J. R. Macdonald, *Impedance Spectroscopy* (Wiley, New York, 1987).
[41]R. J. Sengwa, S. Choudhary and S. Sankhla, Low frequency dielectric relaxation processes and ionic conductivity of montmorillonite clay nanoparticles colloidal suspension in poly(vinyl pyrrolidone)-ethylene glycol blends, *eXPRESS Polym. Lett*. **2**, 800 (2008).
[42]M. Bourguiba, Z. Raddaoui, A. Dhahri, M. Chafra, J. Dhahri and M. A. Garcia, Investigation of the conduction mechanism, high dielectric constant, and non-Debye-type relaxor in $La_{0.67}Ba_{0.25}Ca_{0.08}MnO_3$ manganite, *J. Mater Sci. Mater. Electron* **31**, 11810 (2020).
[43]G. Ioannou, A. Patsidis and G. C. Psarras, Dielectric and functional properties of polymer matrix/ZnO/$BaTiO_3$ hybrid composites, *Compos. A. Appl. Sci. Manuf*. **42**, 104 (2011).
[44]R. Font, J. Portelles and N. Suárez-Almodovar, Frequency-temperature response of ferroelectromagnetic $Pb(Fe_{1/2}Nb_{1/2})O_3$ ceramics obtained by different precursors. III. Dielectric relaxation near the transition temperature, *J. Appl. Phys*. **97**, 1 (2005).
[45]N.Kumar, S. K. Patri, R. N. P. Choudhary *et al*., Frequency-temperature response of a new multiferroic, *Process Appl. Ceram*. **8**, 121 (2014).
[46]K. Prabakar, S. K. Narayandass and D. Mangalaraj, Dielectric properties of $Cd_{0.6}Zn_{0.4}Te$ thin films, *Phys. Stat. Sol*. **199**, 507 (2003).
[47]M. A. Elkestawy, S. Abdel kader and M. A. Amer, AC conductivity and dielectric properties of Ti-doped CoCr1. 2Fe0. 8O4 spinel ferrite, *Physica B* **405**, 619 (2010).
[48]A. M. Farid, H. E. Atyia and N. A. Hegab, AC conductivity and dielectric properties of $Sb_2Te_3$ thin films, *Vacuum* **80**, 284 (2005).
[49]A. A. M. Farag, A. M. Mansour, A. H. Ammar, M. Abdel Rafea and A. M. Farid, Electrical conductivity, dielectric properties and optical absorption of organic based nanocrystalline sodium copper chlorophyllin for photodiode application, *J. Alloys Compd.* **513**, 404 (2012).
[50]R. Amin, K. Samantaray, E. G. Rini, I. Bhaumik and S. Sen, Grain and grain boundary contributions to AC conductivity in ferroelectric $Ba_{0.75}Pb_{0.25}Ti_{1-x}ZrxO_3$ ceramics, *Ceram. Int*. **47**, 13118 (2021).
[51]S. Hajra, M. Sahu, V. Purohit and R. N. P. Choudhary, Dielectric, conductivity and ferroelectric properties of lead-free electronic ceramic: $0.6Bi(Fe_{0.98}Ga_{0.02})O_3$–$0.4BaTiO_3$, *Heliyon* **5**, e01654 (2019).
[52]K. Funke, Jump relaxation in solid electrolytes, *Prog. Solid State Chem*. **22**, 111 (1993).
[53]D. P. Almond, G. K. Duncan, A. R. West, Mobile ion concentrations in solid electrolytes from an analysis of ac conductivity, *Solid State Ion.* **9**, 277 (1983).
[54]G. E. Pike, AC conductivity of scandium oxide and a new hopping model for conductivity, *Phys. Rev. B* **6**, 1572 (1972).
[55]E. Kabir, M. Khatun, R. J. Mustafa, K. Singh and M. Rahman, AC electrical conductivity and dielectric properties of doping induced molecular ferroelectric diisopropylammonium bromide, *Mater. Res. Exp.* **6**, 096306 (2019).

[56]K. C. B. Naidu, V. N. Reddy, T. S. Sarmash, D. Kothandan, T. Subbarao and N. S. Kumar , Structural, morphological, electrical, impedance and ferroelectric properties of BaO-ZnO-$TiO_2$ ternary system, *J. Aust. Ceram. Soc*. **55**, 201 (2019).

[57]A. P. Barranco, Dielectric relaxation and electrical conductivity in ferroelectric ceramic/polymer composite based on modified lead titanate, *J. Appl. Phys*. **102**, 114102 (2007).

[58]A. E. Bachiri, M. E. Hasnaoui, A. Louardi, A. Narjis and F. Bennani, Structural and dielectric studies for the conduction mechanism analyses of lithium-niobate oxide ferroelectric ceramics, *Physica B. Cond. Matt*. **571**, 181 (2019).